

Screen printed thick self-biased, low-loss, barium hexaferrite films by hot-press sintering

Yajie Chen,^{a)} Tomokazu Sakai, Taiyang Chen,^{b)} Soack D. Yoon, Carmine Vittoria, and Vincent G. Harris

Center for Microwave Magnetic Materials and Integrated Circuits, Northeastern University, Boston, Massachusetts 02115 and Department of Electrical and Computer Engineering, Northeastern University, Boston, Massachusetts 02115

(Received 29 December 2005; accepted 6 June 2006; published online 18 August 2006)

BaFe₁₂O₁₉ hexaferrite thick films having high hysteresis loop squareness (M_r/M_s) and low ferromagnetic resonance (FMR) linewidths were processed through the use of a screen printing technique coupled with hot-press sintering. Scanning electron microscopy and x-ray diffraction measurements exhibit strong crystallographic *c*-axis alignment of crystals perpendicular to the film plane. Static magnetic resonance and FMR measurements were performed to determine the effect of the preparation technique on magnetic hysteresis and microwave properties. Hot pressing during sintering produced dense thick films having high squareness (>0.95) and reduced coercivity (~1900 Oe). Of greater importance was the measurement of a minimum peak-to-peak FMR linewidth, 320 Oe at the *U* band, for films ranging in thickness from 100 to 500 μm . Theoretic estimates suggest that such narrow linewidths can be attributed to the reduction in porosity and the improvement in *c*-axis orientation of crystallites in polycrystalline barium ferrite films. As such, hexaferrite materials prepared using this technique offer opportunities in the next generation of self-biased planar microwave devices. © 2006 American Institute of Physics.

[DOI: [10.1063/1.2221527](https://doi.org/10.1063/1.2221527)]

I. INTRODUCTION

The family of magnetoplumbite ferrites, which includes *M*-type barium ferrite BaFe₁₂O₁₉, offers the greatest potential for self-biased microwave and millimeter wave devices that include filters, isolators, and circulators. These devices are essential to the sending, receiving, and manipulation of electromagnetic signals and as a result are integral to applications ranging from wireless communication to radar.¹ The earliest report of self-biased *Y*-junction circulators was in 1974 by Akaiwa and Okazaki, who demonstrated a below-resonance waveguide device at 77 GHz.² Since that time many attempts have been made to achieve self-biased microwave/millimeter devices.³ During the early 1990s, Weiss *et al.* carried out work on self-biased above-resonance (31 GHz) devices.^{4,5} In addition, there are also high-power applications for self-biased ferrite in quasioptical circulators based on Faraday rotation of linear polarized radiation that would benefit from an improved *c*-axis aligned ferrite material. Transmission and reflection versions were demonstrated with conventional ferrite,^{6,7} and a self-biased transmission device was later demonstrated by Webb.⁸ However, today's commercial circulators are still relatively large because of the need for permanent magnets that provide the necessary external magnetic biasing field. The use of these magnets hinders efforts to reduce the size of these devices and add expense in processing and assembly.⁹

A promising way to omit the need for the permanent

magnet is to utilize the hexagonal Ba ferrite material that has a high effective internal field as a result of strong crystalline anisotropy. Such a self-biased material remains magnetized even after an applied magnetic field is removed. This has been a long-standing problem whose solution will have a wide ranging impact on the field of microwave magnetic devices. An ideal ferrite for circulator applications possesses the following properties: thicknesses greater than 300 μm , self-biased (i.e., high remanent magnetization), low microwave losses ferromagnetic resonance (FMR) linewidths typically less than 500 Oe, and the magnetization vector aligned perpendicular to the plane of the device.¹⁰

There have been many efforts to produce ferrite films for microwave device applications over the past several years.¹¹ Pulsed laser deposition (PLD) was used to produce high quality Ba hexaferrite films on various substrates.¹² The disadvantages of this approach include a limited thickness of a few microns, low growth rates, small surface area, and a low remanence magnetization (i.e., no potential for self-biasing). Liquid phase epitaxy (LPE) has been used to process thick (~100–200 μm) films on some select microwave substrates.¹³ The LPE films exhibit low microwave loss but small remanent magnetization. The LPE process is also limited to relatively small size substrates. Conventional bulk compacts¹⁴ prepared in a magnetic field have demonstrated self-biased properties at large thicknesses (i.e., millimeters). However, the alignment of grains in bulk materials depends mostly on utilization of a high magnetic field, except for using a thermomechanical process without a magnetic field.¹⁵ In addition, the conventional bulk ceramic technique is limited in sample size since bulk compacts often need to

^{a)} Author to whom correspondence should be addressed; electronic mail: y.chen@neu.edu

^{b)} Internship student, Brookline High School, Brookline, MA 02445.

be cut and polished in order to obtain small disks required in microwave applications. An extra mechanical process not only increases costs but also may give rise to changes in physical properties. Typically, the microwave losses are relatively high for the sintered compacts.

Thick film technology, e.g., the screen printing (SP) technique, is capable of producing films several 100 μm thick.¹⁶ In the modern electronics industry, this screen printing technique has been applied to produce thick film circuits and sensors.¹⁷ However, this technique has not been extended to fabricate textured BaM thick films prior to our efforts.^{18,19} In previous studies, screen printed BaM ferrite thick films had large FMR linewidths (ΔH) of about 1000 Oe. Although much smaller than values reported for polycrystalline BaM materials, (~ 2000 Oe),² such FMR linewidths remain too large for most microwave device applications. Both experiment and theoretic calculations presented here indicate that the large linewidths arise predominantly from porosity in the BaM films. Clearly, if the screen printing technique can be refined to reduce pores it will offer unique potential to produce practical BaM thick films (i.e., thick, self-biased, low loss) in a cost effective and scalable process.

The present paper addresses the fabrication of dense textured BaM thick films by screen printing combined with a hot-press (HP) sintering technique. We have developed a processing scheme in which Ba hexaferrite is produced having thicknesses up to 500 μm , a high remanent magnetization (i.e., as high as 96% of saturation values), perpendicular magnetic anisotropy (magnetization aligned perpendicular to the film plane), and low microwave losses (ferromagnetic resonance linewidth of ~ 320 Oe). These properties make these films ideal for use in self-biased planar microwave circulators.

II. EXPERIMENT

A. Sample preparation

The processing technique makes use of a screen printing technology where a paste, consisting of BaM particles suspended in a binder (B-75000, Ferro), is spread over a stencil onto a suitable microwave substrate, e.g., 0.25 mm thick alumina (supplied by Accumet Engineering Corp.) [see Fig. 1(a)]. The stencil was used to print circular disks of ferrite material at a desired thickness that were mostly powder (>70 wt % ferrite) with little binder. The ultimate thickness of the sintered films was approximately 80%–90% of the as-printed thickness (i.e., the stencil thickness). A blade was required to maintain an even thickness across the stencil area.

The starting powders were prepared by conventional ceramic processing. After repeated solid state reaction of the initial oxide reagents ($\text{BaCO}_3:\text{Fe}_2\text{O}_3=1:6$) at 1250 $^\circ\text{C}$ for 15 h, the powders were reduced to 1.0–1.5 μm diameter particles by ball milling. The screen printing paste typically consisted of 25.5 wt % binder, 2.5 wt % glass frit, and 72 wt % barium hexaferrite powder.

The resulting film was subjected to a magnetic field (~ 8000 Oe) aligned perpendicular to the film plane during

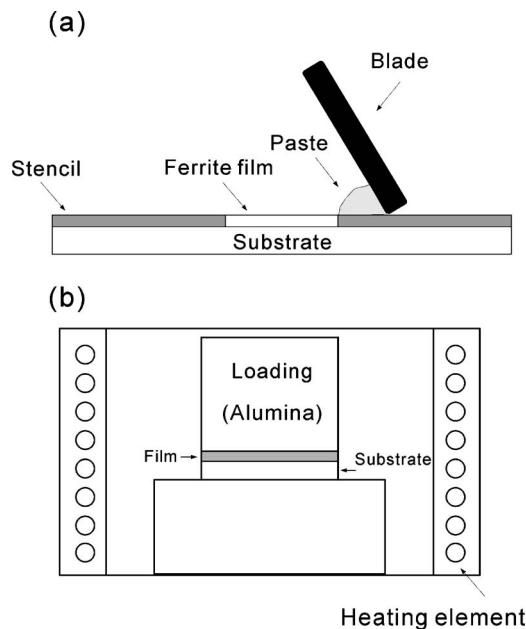


FIG. 1. (a) Sketch detailing the screen printing apparatus. (b) Sketch of the hot-press sintering procedure for screen printed BaM ferrite thick films.

the first heat treatment (150–250 $^\circ\text{C}$, 1–20 min). The magnetic field acting upon the still wet film aligned the BaM particles with respect to the magnetic field direction. This alignment forced the c axes of the hexaferrite particles, and subsequently the magnetization, to align along the direction perpendicular to the film plane. This low temperature heat treatment acted to vaporize the binder and fix the orientation of the particles. The film then underwent a hot pressing during the second sintering heat treatment in air to temperatures ranging from 900 to 1300 $^\circ\text{C}$ at times ranging from 1 to 12 h. The hot pressing was performed by placing a load (e.g., an alumina block) on top of the film. A typical load ranged from 1 to 5 MPa. This is illustrated in Fig. 1(b). This hot-pressing process is an essential step in improving the film density and reducing the microwave losses of the film. A third heat treatment was sometimes required to complete the sintering of the film and to reduce strain. The final film had an area of 1 cm^2 and a thickness of 200–500 μm . The flow chart of the process is illustrated in Fig. 2.

B. Measurement method

The screen printed BaM films were characterized in terms of their structural, magnetic, and microwave properties. The degree of crystallographic orientation was obtained from Philips X'pert PRO x-ray diffraction (XRD) measurements using a $\text{Cu K}\alpha$ radiation source. The morphology of the films was examined using a Hitachi S-4800 ultrahigh resolution scanning electron microscope (SEM). The thickness of the films was determined using a step profilometer. Static magnetic properties were measured using a vibrating sample magnetometer (VSM) and microwave magnetic properties of the BaM films were characterized by the out-of-plane FMR measurements using a shorted waveguide. In the FMR measurements, the external magnetic field was swept at a fixed frequency using a TE_{10} mode propagation in

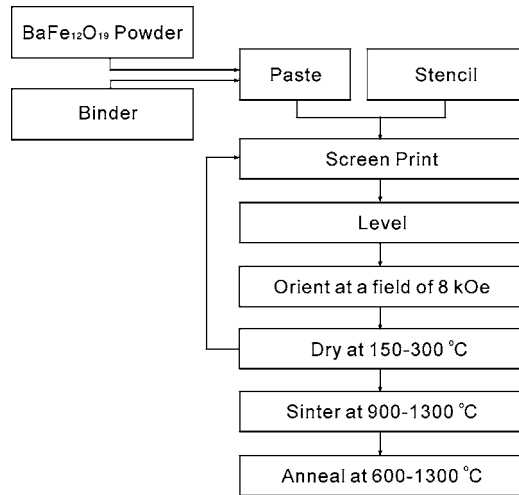


FIG. 2. Processing flowchart for screen printed oriented BaM ferrite films.

a U band (40–60 GHz) waveguide. Since the magnetic easy axis was perpendicular to the film plane, we applied the external magnetic field H_0 parallel to the easy direction, i.e., perpendicular to the film plane. Thus, the microwave magnetic field \mathbf{h} was applied in the plane of the BaM film.

III. RESULTS AND DISCUSSION

A. Microstructure and sintering kinetics

XRD patterns of the screen printed BaM thick films are shown in Fig. 3. We observed a single phase $\text{BaFe}_{12}\text{O}_{19}$ for all samples including the initial ferrite powder and the sintered films. No peaks arose from the film substrate, sample holder, or mounting clay. Figure 3(a) indicated that reflections of (200), (226), (405), and (107) were still observed besides the predominant (00 l) peaks. This was reasonable in that the as-printed film had a low squareness ($SQ = M_r/M_s$) of about 0.6 before sintering. However, XRD analysis showed enhanced (00 l) intensities after the film underwent a normal sintering above 1000 °C [see Fig. 3(b)]. We only observed strong reflections of (104) and (108) and a low intensity (1013) peak. More importantly, after the screen printed film underwent a hot-press sintering, the resultant XRD pattern exhibited only (10 l) and (20 l) reflections where l was an even integer. Intensities of the other peaks decreased significantly. The uniaxial HP sintering further enhanced the texture, as is illustrated in Fig. 3(c).

Figure 4(a) shows a SEM micrograph of the BaM thick film before sintering. The as-printed film had a microstructure of loosely arranged grains that were largely isotropically aligned. Some of the raw particles have had a high aspect ratio (i.e., hexagonal platelets) that would ultimately provide crystallographic textured thick films. Figure 4(b) is a SEM micrograph of the film surface after normal sintering. Although the density of the film increased, there existed large pores having sizes between 0.5 and 2 μm . The grain size ranged from 1.5 to 4.0 μm . It is worth noting that the number and size of pores were greatly reduced after the screen printed film was subjected to the HP sintering process. This is illustrated in Fig. 4(c). In that case, the film had low porosity and small pores typically with diameters of 0.3 and

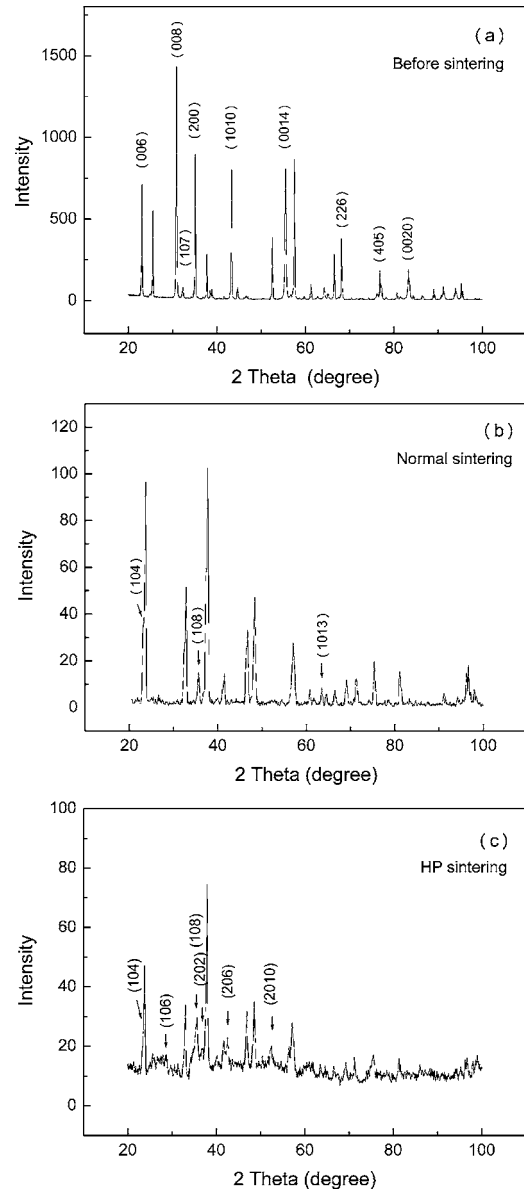


FIG. 3. XRD patterns for BaM ferrite thick films: (a) as-printed thick film before sintering, (b) film after normal sintering at 1200 °C, and (c) film after hot-press sintering at 1200 °C.

1.0 μm . The average grain size ranged from 2 to 3 μm . It was hard to identify large pores similar to those observed in normal sintered films. A SEM image of a fractured surface in cross section of the HP sintered film is depicted in Fig. 4(d). The cross-section micrograph clearly illustrates a highly oriented layered microstructure of grains believed to be the side view of stacked hexagonal crystals. This interpretation is consistent with the XRD analysis. Comparison of Figs. 4(b)–4(d) indicates that appreciable densification and grain growth occurred during HP sintering. Moreover, the grains grew mostly along the film plane (i.e., basal plane of the crystals), which was in accord with XRD results in Fig. 3(c). It is postulated that during the HP sintering process the initial high-aspect-ratio BaM platelets acted as seeds to promote further grain growth and texturing. During the sintering process the fine particles were assimilated thereby reducing the nontextured component of the film microstructure. As a re-

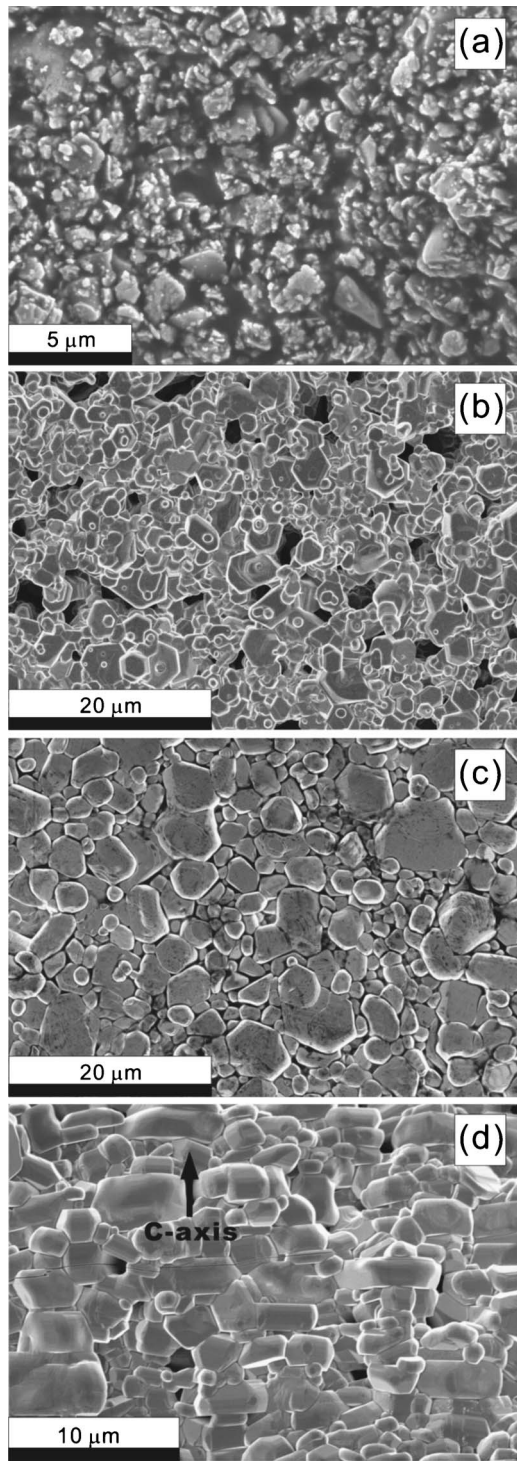


FIG. 4. SEM micrographs for BaM ferrite thick films: (a) as-printed thick film surface before sintering, (b) film surface after normal sintering at 1200 °C, (c) film surface after hot-press sintering at 1200 °C, and (d) cross section of the film after hot-press sintering at 1200 °C.

sult of XRD and SEM measurements, it is concluded that the texturing and density were enhanced by the high temperature sintering process, especially during the hot-press sintering process.

During sintering, two principle microstructural changes occurred: porosity reduction (i.e., densification) and grain growth. The driving force for this densification and grain growth is the lowering of the film's total free energy by the

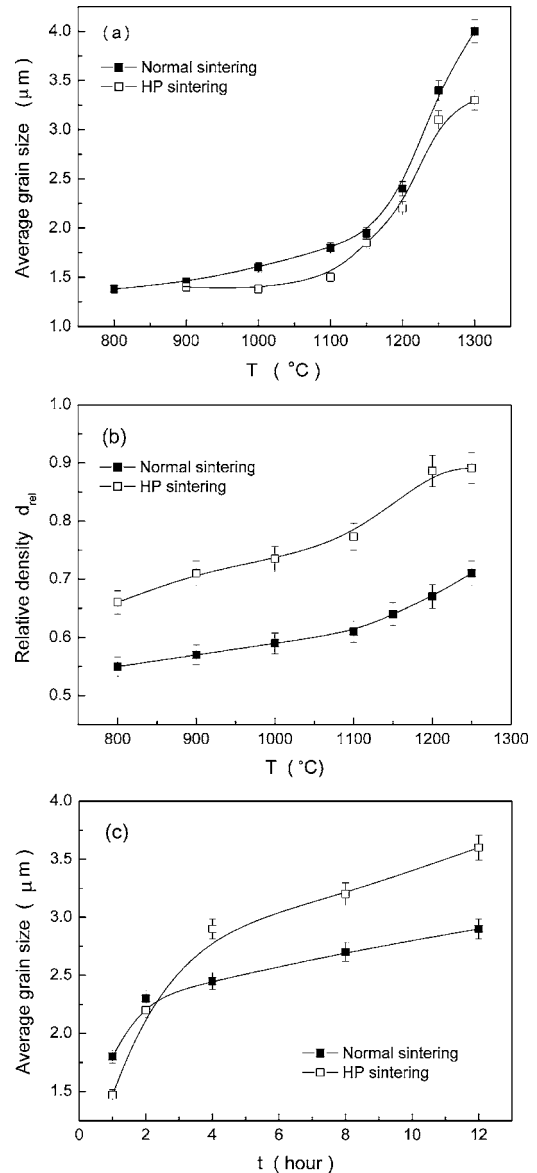


FIG. 5. Comparison of two samples processed by normal and hot-press sintering. (a) Temperature dependence of grain size for BaM films at a sintering time of 2 h. (b) Temperature dependence of the relative density d_{rel} for BaM films after sintering for 2 h. (c) Variation of grain size with sintering time at 1200 °C.

reduction of the free surface of the particles. It appears that HP sintering increases grain growth at elevated temperatures, especially above 1150 °C [see Fig. 5(a)]. The results also indicate that the HP sintering can impede grain overgrowth to some extent. The normal sintering produced larger grains than the HP sintering for the highest sintering temperatures. The primary goal was the elimination of pores and increased density, rather than minimizing grain growth. Figure 5(b) compares the normal and HP sintered films when the relative density (d_{rel}), defined as the ratio of measured to theoretical, was varied with sintering temperature. Clearly, density depended strongly on the temperature used in HP sintering, particularly for $T > 1000$ °C. The films largely retained a smooth morphology and did not develop isotropic polycrystalline BaM crystallites.

Since the normal sintering process depends on the capillary pressures resulting from the surface energy to provide

the driving force for densification, the shrinkage rate of the large pores was impractically slow. This is due to the small driving force and the long diffusion distance in screen printed films. Importantly, the large pores shrank at $T < 1000$ °C without a corresponding grain growth [see Fig. 5(a)]. With the increase in the grain boundary mobility, the grain growth first occurs near the pore surface. This results in merging some neighboring grains and reducing the number of neighboring grains. The large pores, surrounded by the hexagonal grains, thereby shrink and even disappear.

The aim of the hot-pressing technique is to apply an external pressure to the film at an elevated temperature rather than relying entirely on densification by the capillary action. In general, densification can be obtained at temperatures below which extensive grain growth or secondary recrystallization occurs. It was suggested²⁰ that minimum FMR linewidths could be obtained by applying the hot-pressing technique to maximize the density of the ferrite films. Since the grain-growth process is largely insensitive to pressure, hot-pressing sintered ferrites at moderate temperatures allow fabrication of the samples with high-density and relatively small grains. The hot-pressing process can be described in terms of following kinetic equation:²¹

$$\frac{d(\ln d_{\text{rel}})}{dt} = A \left(\frac{D}{kT} \right) (G^{-p}) (\sigma_{\text{eff}})^n, \quad (1)$$

where d_{rel} is relative density, A is a constant, D is the diffusion coefficient, G is the grain size, and σ_{eff} is effective stress. The n and p are the stress exponent and grain size exponent, respectively. Equation (1) indicates that the rate of change in density is inversely proportional to the sintering temperature and more so grain size due to $p \approx 2$.²² At the same time, the kinetic equation gives a critical clue, that is, the effective stress serves to produce dense materials due to $1 < n < 2$ in the low stress situation.²²

Figure 5(c) presents the dependence of grain size with sintering time for both normal and HP sintered films. It is reasonable that the grains grow slowly after 4 h due to the presence of a number of large grains having low surface energy. Alternatively, the HP sintering has a great increase in grain size after just 2 h. This suggests that the densification process can be fulfilled at a shorter time during the HP sintering. Hence, the experimental results are in agreement with the predictions from Eq. (1).

B. Magnetic properties

As in the case of the microstructural properties, the changes in the static magnetic properties of the films as a function of sintering conditions were different for the films sintered by the normal and HP processes. Static magnetic properties of the films were obtained from VSM measurements with an external field of 12.5 kOe applied parallel and perpendicular to the film plane. Figure 6 shows the variation of the saturation magnetization with temperature in films processed by normal sintering. The $4\pi M_s$ increased monotonically with temperature from 800 to 1250 °C, which was in accord with the sintering temperature dependence of density in the ferrite film. Both coercivity and squareness of

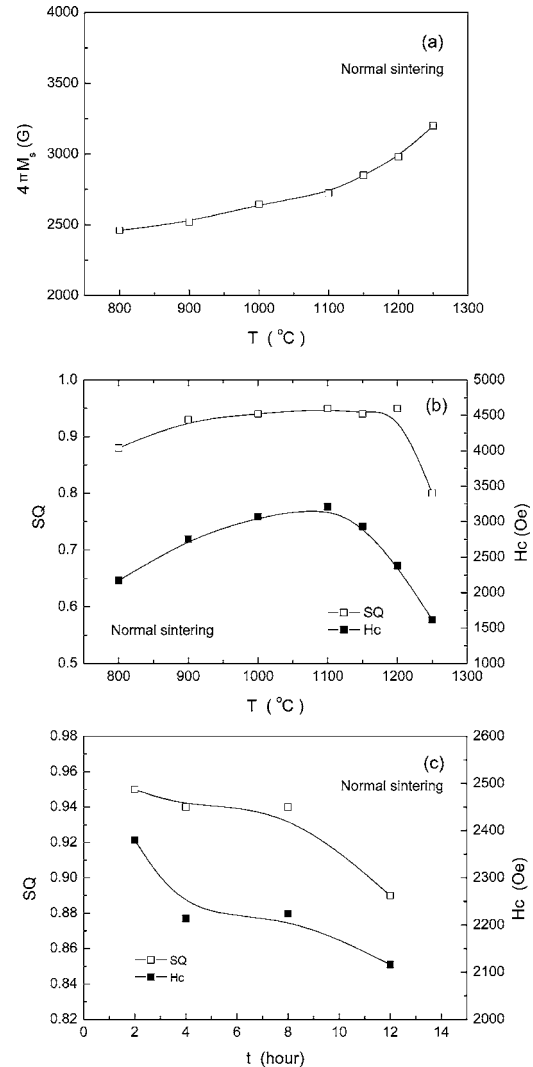


FIG. 6. Dependence of magnetic properties of BaM films on sintering condition by normal sintering. (a) Variation of saturation magnetization with sintering temperature. (b) Variation of squareness and coercivity with sintering temperature. (c) Variation of squareness and coercivity with sintering time.

the film plane, i.e., along the magnetic easy direction, depended strongly on sintering temperature, shown in Fig. 6(b). The SQ increased gradually until $T=1200$ °C, and subsequently decreased quickly for $T>1200$ °C. The coercive field was observed to increase with temperature due to the reduction in pore density for $T<1100$ °C, whereas the grain growth led to a reduction in H_c for $T>1100$ °C. The coercive field exhibited a maximum at 1100 °C. This interpretation is supported by the microstructural measurements presented in Fig. 5(a).

Squareness and coercivity are greatly sensitive to microstructure, that is, the porosity, grain structure, and phase purity. Pores and grain boundaries effectively pin magnetic domain walls and thereby give rise to increased coercivity and loop squareness. Thus, increasing the sintering time to 12 hours resulted in a reduction in both SQ and H_c , which is attributed to the presence of multidomains in the individual grains [see Fig. 6(c)].

Figures 7(a)–7(c) illustrate magnetization, SQ, and H_c measured along the easy axis as functions of sintering tem-

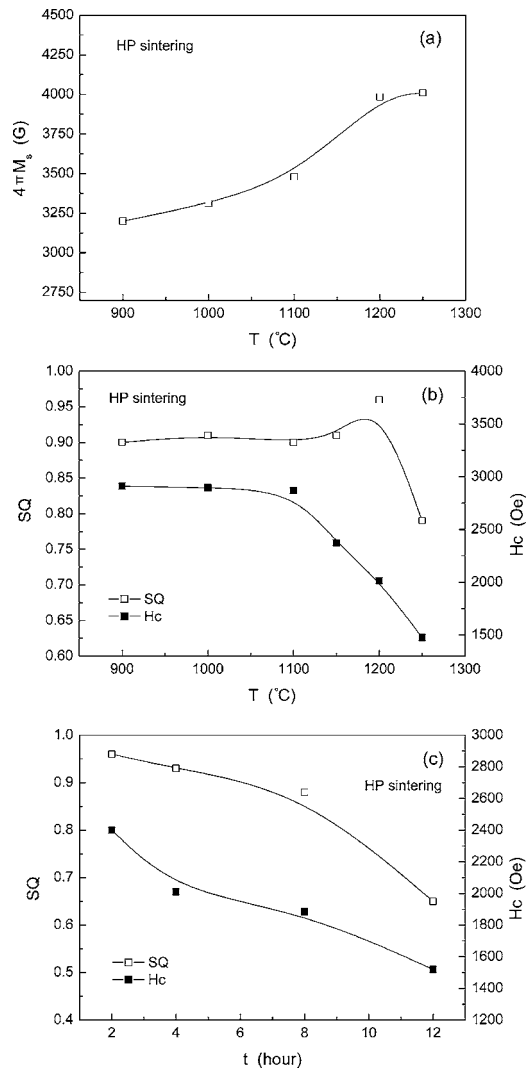


FIG. 7. Dependence of magnetic properties for BaM thick films on sintering condition by hot-press sintering. (a) Variation of saturation magnetization with sintering temperature. (b) Variation of squareness and coercivity with sintering temperature. (c) Variation of squareness and coercivity with sintering time.

perature and soak time used in the HP sintering process, respectively. The dependence of magnetic properties on sintering parameters is similar to those in normal sintering. However, one difference is that the apparent shrinkage of pores in the HP sintering begins at a relatively low temperature. Additionally, the average saturation magnetization is enhanced by 30% for samples prepared by the HP sintering compared to those prepared by the normal sintering. This is reasonable in that the film density is sensitive to an external pressure in the sintering process. Among these samples, an optimized thick film had $4\pi M_s=4000$ G, $SQ=0.96$, and $H_c=1935$ Oe. These results were expected to give rise to a narrow FMR linewidth. In order to further the effect of texture (anisotropy) in the films, Fig. 8 shows magnetic hysteresis loops of the film magnetized along the easy and hard axes when different soak times were applied in the sintering process. Since the BaM ferrite films were fabricated for use in self-biasing microwave devices, the remanence (or squareness) and the coercive field are two important parameters. Squareness is directly responsible for the self-biasing prop-

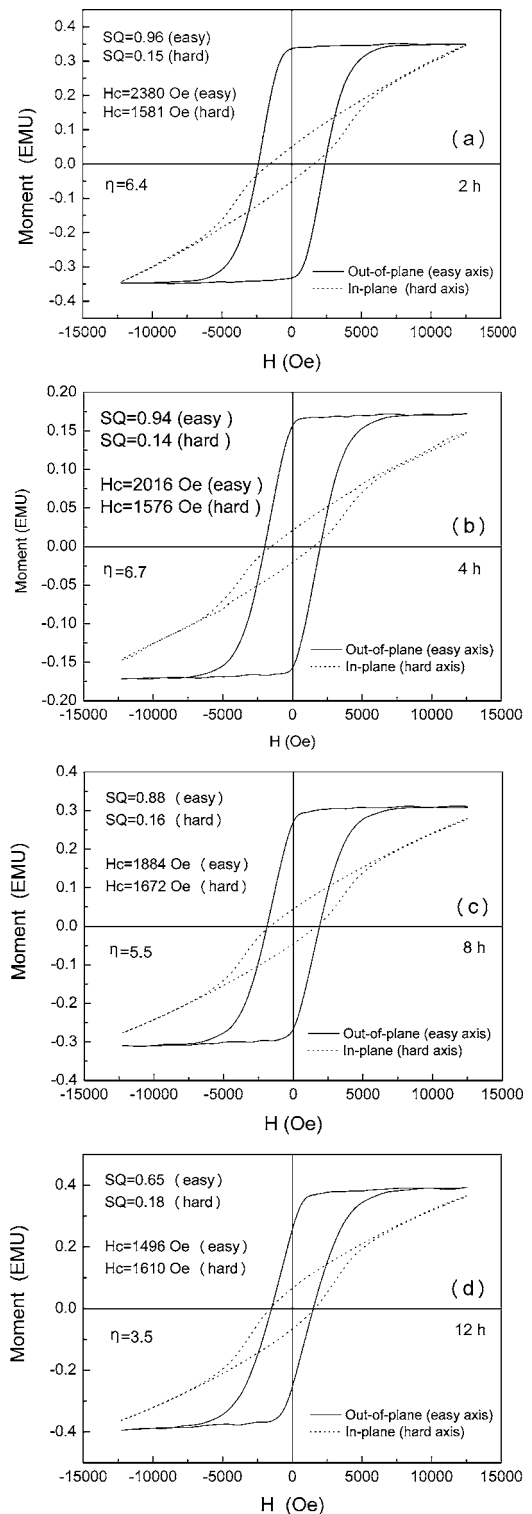


FIG. 8. Magnetic hysteresis of hot-press sintered BaM films for different sintering times: (a) 2 h, (b) 4 h, (c) 8 h, and (d) 12 h.

erties, whereas a low coercive force is assumed to be required for narrow FMR linewidths.²³ Here, we introduce a parameter $\eta=SQ(\text{easy})/SQ(\text{hard})$ to describe how different the magnetic anisotropy was out of plane from in plane so that the degree of crystallographic texture could be evaluated. Figures 8(a)–8(d) illustrate that the SQ and H_c , measured along the easy axis, were reduced from 0.96 and 2380 Oe to 0.65 and 1610 Oe with HP sintering soak times

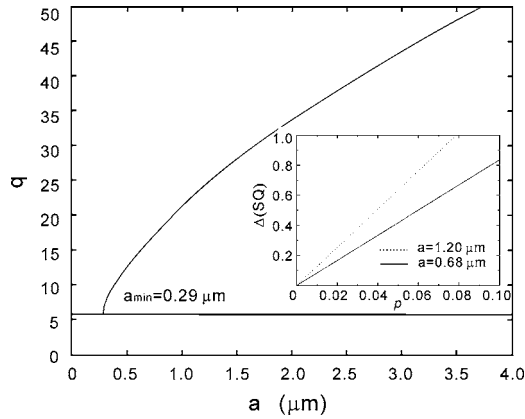


FIG. 9. Effect of parameter q on grain size for $(K_1/A)^{1/2} = 2.57 \times 10^6 \text{ cm}^{-1}$. The inset shows that the reduction of $\Delta(\text{SQ})$ is a function of porosity for films produced by normal sintering (solid line) and hot-press sintering (dashed line).

of 2–12 h, respectively. The parameter η varied from 6.4, 6.7, 5.5, and 3.5, corresponding to soak times of 2, 4, 8, and 12 h, respectively. From this, a 4 h HP sintering was found to produce the strongest magnetic anisotropy and texture out of film plane. This is expected to give rise to a small broadening of the FMR linewidth due to variations in anisotropy field.²⁴

Magnetic hysteresis of polycrystalline materials is acutely sensitive to the presence of nonmagnetic entities, including pores, secondary phases, and grain boundaries. The remanent magnetization is determined to a large extent by the nucleation of reverse or 90° Néel spike domains about a pore or grain boundary. The size of any spike domains will directly contribute to a reduction in squareness. Therefore, the reduction in squareness by porosity, $\Delta(\text{SQ})$, might be estimated by calculating the volume of the spike domains from a simple formula,²⁵

$$\Delta(\text{SQ}) = (\pi/6)qp, \quad (2)$$

where p is the fraction of porosity ($p = na^3$). If $q = 2l/a \gg 1$, where l is the length of the spike domain and a is the edge dimension of the cubic pore, the q is approximately given by

$$q^2 \approx (K_1/A)^{1/2}a(\ln 2q - 2). \quad (3)$$

K_1 and A are the first-order anisotropy constant and the exchange constant, respectively. For BaM material, we have $A = 0.5 \times 10^{-6} \text{ erg cm}^{-1}$ (Ref. 26) and $K_1 = 3.3 \times 10^6 \text{ erg cm}^{-3}$.²⁷ For a value of $(K_1/A)^{1/2} = 2.57 \times 10^6 \text{ cm}^{-1}$, the dependence of q on a can be calculated by iteration, shown in Fig. 9. It should be pointed out that in this case a minimum pore size and parameter q value were $a_{\min} = 0.29 \mu\text{m}$ and $q_{\min} = 6.1$. This implies that any pore less than this critical size is unable to nucleate spike domains. A rough estimate of a HP sintered sample indicated that the reduction in SQ was about 0.05 due to porosity, assuming an average pore size $a = 0.68 \mu\text{m}$, and $p = 0.006$ from Figs. 4(c) and 4(d). Here we only considered the pores having sizes larger than the critical dimension to contribute to squareness. The estimated $\Delta(\text{SQ}) = 0.051$ (inset of Fig. 9) is in agreement with VSM measurements, i.e., $\text{SQ} = 0.95$. We suggest that the estimate from theory should be larger than measured values

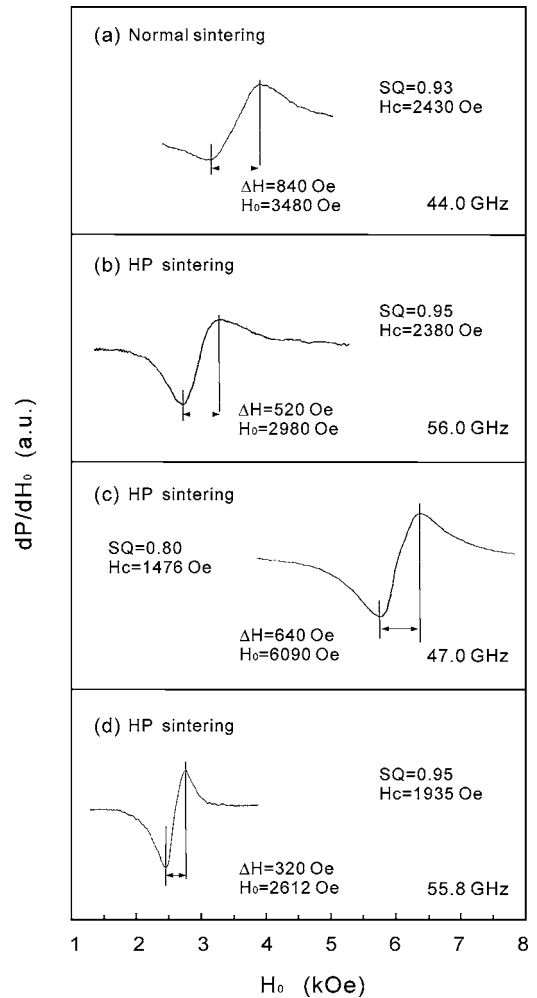


FIG. 10. FMR measurements for screen printed films sintered by different sintering techniques: (a) normal sintering at 1200°C , 2 h; (b) hot-press sintering at 1200°C , 2 h; (c) hot-press sintering at 1250°C , 4 h; and (d) hot-press sintering at 1200°C , 4 h, followed by an annealing at 1000°C for 6 h.

since nonaligned grains contribute to the measured squareness values. A maximum angular distribution of $\sim 20^\circ$ of c -axis grains was observed in the best oriented film ($\text{SQ} = 0.96$)

Subsequently, we analyzed another sample produced by normal sintering. Taking parameter $a = 1.20 \mu\text{m}$, and $p = 0.019$ as deduced from the SEM image in Fig. 4(b), the calculation gave rise to $\Delta(\text{SQ}) = 0.233$, which was not in agreement with measured values ($\text{SQ} = 0.90\text{--}0.93$) in this case. The difference may be due to neighboring pores that are far enough apart that the interaction between closure domains might be negligible. Another possibility is that stress in the film was responsible for some portions of the squareness, depending on the sign and magnitude of $\sigma\lambda/K_1$.²⁸

C. FMR measurement

As mentioned above, one of the aims of this research was to produce practicable hexaferrite thick films with reasonable ferromagnetic resonance linewidth ($< 500 \text{ Oe}$) at $\sim 50 \text{ GHz}$. Figure 10 shows typical FMR measurements for the samples produced by the different sintering techniques.

The peak-to-peak derivative linewidth (ΔH) was obtained from the sample produced by normal sintering, illustrated in Fig. 10(a). The thick film had a broad linewidth of 840 Oe at an external field H_0 of 3480 Oe, corresponding to a high SQ of 0.93 and coercivity of 2430 Oe. We estimate that about 600–700 Oe of the measured ΔH (=840 Oe) resulted from porosity.

Figures 10(b)–10(d) show derivative FMR curves for the samples prepared by different HP sintering conditions. The HP sintered films clearly have lower microwave losses, compared with the normal sintered samples. Figures 10(b) and 10(c) exhibit linewidths of 520 and 640 Oe, respectively. The small difference in ΔH between the two samples arose from several factors: (1) squareness, (2) coercivity, and (3) resonance frequency. Importantly, the film in Fig. 10(c) required a large external field ($H_0=6090$ Oe) to excite FMR due to its small SQ (=0.80), whereas another film with high SQ (=0.95) in Fig. 10(b) only needed a resonant external field of ~ 2980 Oe. A squareness of 0.80 may be unsuitable for self-biasing devices, but the linewidth of the film was comparable to that of the best of the normal sintered films with SQ=0.93 [see Fig. 10(a)]. Detailed studies suggest that the film (b) retained a high crystallographic texture in that the XRD patterns illustrated good texture of grains and the VSM measurements had a low SQ of 0.14 for the magnetic field aligned along the film plane (i.e., the hard axis). As a result, the reduction in SQ may be explained in terms of the formation of a multidomain structure in the individual grains.

Here, an emphasis is placed on the need to maintain the largest possible coercive field in order to minimize shape demagnetizing effects of a planar geometry for the c -axis grain aligned thick films. This implies that the material should have a microstructure of uniformly small grains. However, it is challenging to optimize both coercivity and FMR linewidth simultaneously, since the microstructure of fine grains is usually responsible for a large FMR linewidth.²³

An optimized film fabricated by HP sintering exhibited the narrowest FMR linewidth [see Fig. 10(d)]. Due to high SQ (=0.95) and appropriate coercive field (1935 Oe), the film yielded a linewidth of 320 Oe at an external field of 2612 Oe and a resonant frequency of 55.8 GHz. In polycrystalline materials, FMR linewidths result predominantly from extrinsic contributions,²⁹ i.e., including porosity, impurities, grain boundaries, and randomly oriented grains. Here, we estimate qualitatively the nonuniform contributions to the FMR linewidth in our samples in terms of the following equation:^{30,31}

$$\Delta H = 1.8\pi \frac{\langle H_F^2 \rangle}{4\pi M} J, \quad (4)$$

where $\langle H_F^2 \rangle$, a mean square fluctuation field, is responsible for both the anisotropy and porosity broadening effects in the materials. J is a shape factor given by

$$J = \frac{1}{6} \left(\frac{\omega_0}{\omega_1} \right) \left(\frac{\omega_1 \omega_M}{\omega_2^2 - \omega_0^2} \right)^{1/2} \left[1 + 5 \left(\frac{\omega_0^2 + \omega_1^2}{2\omega_0 \omega_1} \right) \right]. \quad (5)$$

Schlömann²³ calculated $\langle H_F^2 \rangle_{\text{anis}}$ and $\langle H_F^2 \rangle_{\text{poros}}$ and rewrote Eq. (2) as follows:

$$\Delta H = \Delta H_{\text{anis}} + \Delta H_{\text{poros}} = 1.08J \left(\frac{H_A^2}{4\pi M} \right) + 0.502J4\pi Mp, \quad (6)$$

where H_A is the anisotropy field equal to $2|K_u|/M$ and p is the porosity in the material. Assuming porosity $p=0.1$ and $J=0.94$ (demagnetizing factor of $N_Z=0.9$ and $N_i=0.05$), we obtained $\Delta H_{\text{anis}}=61$ Oe and $\Delta H_{\text{poros}}=213$ Oe. Here ΔH_{anis} was derived from the assumption of randomly oriented anisotropic axes, and thereby the estimate should be greater than the actual value in a highly oriented sample. Given an intrinsic linewidth of about 30 Oe, that was obtained from our measurement of single crystal of BaM films,⁶ we calculated a total linewidth of about 304 Oe for the thick oriented film samples. This estimate is in reasonable agreement with the measured value of 320 Oe, as presented in Fig. 10(d). We believe that further reduction in linewidth is possible by enhancing texture and the further reduction of pores. Therefore, we conclude that eliminating porosity is a critical step in obtaining narrow linewidths in oriented polycrystalline ferrite materials. Nevertheless, a large part of the FMR linewidth is probably caused by the inhomogeneous broadening from the high magnetocrystalline anisotropy of the misaligned grains even in the case of very low porosity. However, a linewidth of a few hundred oersted (e.g., 200–300 Oe) may not be necessarily a problem as long as the device operates far from the FMR frequency.

IV. CONCLUSION

We have developed a processing scheme for the fabrication of thick films of Ba hexaferrite having high remanent magnetization, low microwave losses, and magnetic anisotropy perpendicular to the film plane. The remanent magnetization remains high (SQ>0.95), thereby eliminating the need for a biasing magnet for self-biasing microwave device applications. The process also allows for the synthesis of thick films in the hundreds of micron to millimeter range. These thicknesses offer the needed filling factor for device operation. The process allows for the deposition of thick films over large surface areas making it suitable for batch processing of devices or applications that require large area substrates. A unique hot-press sintering technique is applied to densify screen printed films resulting in films having low FMR linewidths (~ 320 Oe) at the U band. This process is comparatively inexpensive compared with other film processing schemes. We believe that our results will serve as impetus for future work in self-biased ferrite materials for microwave devices.

ACKNOWLEDGMENTS

This work was supported by DARPA Grant No.HR0011-05-1-0011 and ONR Grant No.N00014-05-10349.

- ¹H. L. Glass, Proc. IEEE **76**, 151 (1988).
- ²Y. Akaiwa and T. Okazaki, IEEE Trans. Magn. **10**, 374 (1974).
- ³J. D. Adam, L. E. Davis, G. F. Dionne, E. F. Schloemann, and S. N. Stitzer, IEEE Trans. Microwave Theory Tech. **50**, 721 (2002).
- ⁴J. A. Weiss, N. G. Watson, and G. F. Dionne, IEEE MTT-S Int. Microwave Symp. Dig. **1**, 145 (1989).
- ⁵J. A. Weiss, N. G. Watson, and G. F. Dionne, Applied Microwave Magazine, Fall 1990, p. 74.
- ⁶G. F. Dionne, J. A. Weiss, and G. A. Allen, IEEE Trans. Magn. **24**, 2817 (1988).
- ⁷B. Lax, J. A. Weiss, N. W. Harris, and G. F. Dionne, IEEE Trans. Microwave Theory Tech. **41**, 2190 (1994).
- ⁸M. R. Webb, Int. J. Infrared Millim. Waves **12**, 45 (1991).
- ⁹M. A. Tsankov and L. G. Milenova, J. Appl. Phys. **73**, 7018 (1993).
- ¹⁰V. G. Harris, C. Vittoria, F. J. Rachford, and Y. Chen, U.S. Patent No. 60/714444 (pending).
- ¹¹V. G. Harris *et al.*, J. Appl. Phys. **99**, 08M911 (2006).
- ¹²S. D. Yoon, S. A. Oliver, and C. Vittoria, J. Appl. Phys. **91**, 7379 (2002).
- ¹³S. G. Wang, S. D. Yoon, and C. Vittoria, J. Appl. Phys. **92**, 6728 (2002).
- ¹⁴G. F. Dionne and J. F. Fitzgerald, J. Appl. Phys. **70**, 6140 (1991).
- ¹⁵L. A. Brisette and E. Underhill, 101st Annual Meeting & Exposition of the American Ceramic Society, Indianapolis, Indiana, 1999 (unpublished).
- ¹⁶H. Altenburg, J. Plewa, G. Plesch, and O. Shpotyuk, Pure Appl. Chem. **74**, 2083 (2002).
- ¹⁷K. Arshaka, K. Twomey, and D. Egan, Sensors **2**, 50 (2002).
- ¹⁸Y. Chen, A. L. Geiler, T. Sakai, S. D. Yoon, C. Vittoria, and V. G. Harris, J. Appl. Phys. **99**, 08M904 (2006).
- ¹⁹Y. Chen, A. T. Sakai, T. Chen, S. D. Yoon, L. Geiler, C. Vittoria, and V. G. Harris, Appl. Phys. Lett. **88**, 062516 (2006).
- ²⁰A. V. Nazarov, D. Ménard, J. J. Green, C. E. Patton, G. M. Argentina, and H. J. Van Hook, J. Appl. Phys. **94**, 7227 (2003).
- ²¹R. K. Bordia and R. Raj, J. Am. Ceram. Soc. **71**, 302 (1988).
- ²²C. J. Ting and H. Y. Lu, Acta Mater. **47**, 817 (1999).
- ²³T. Inui and N. Ogasawara, IEEE Trans. Magn. **13**, 1729 (1977).
- ²⁴D. R. Franklin, A. J. Pointon, and R. C. L. Jenkins, J. Phys. D **29**, 1268 (1996).
- ²⁵G. F. Dionne, J. Appl. Phys. **40**, 431 (1969).
- ²⁶D. J. Craik, *Structure and Properties of Magnetic Materials* (Pion Limited, London, 1971).
- ²⁷C. A. Carosella, D. B. Chrisey, P. Lubitz, J. S. Hotwitz, P. Dorsey, R. Seed, and C. Vittoria, J. Appl. Phys. **71**, 5107 (1992).
- ²⁸G. F. Dionne, IEEE Trans. Magn. **5**, 596 (1969).
- ²⁹M. Sparks, J. Appl. Phys. **36**, 1570 (1965).
- ³⁰S. Geschwind and A. M. Clogston, Phys. Rev. **108**, 49 (1957).
- ³¹E. Schlömann, J. Phys. Chem. Solids **6**, 242 (1958).